The University of Queensland
Australia

gciQ Global Change Institute

July 2016
DISCUSSION PAPER No. 6

Projecting Solar PV Yield of the Solar Array Installed at UQ Gatton Campus Using NREL's SAM Model

Prepared by Phillip Wild, PhD
Postdoctoral Research Fellow
Global Change Institute
The University of Queensland

PROJECTING SOLAR PV YIELD OF THE SOLAR ARRAY INSTALLED AT UQ GATTON CAMPUS USING NREL'S SAM MODEL

By Phillip Wild

Email: p.wild@uq.edu.au

Telephone: work (07) 3346 1004; Mobile 0412 443 523

Version 3 – 19 July 2016

Abstract

The viability of utility scale solar PV farms will depend critically upon the annual production of such farms. A crucial determinant of solar PV yield will be prevailing solar irradiance and weather conditions. In Australia, the combined effects of weather relating to solar irradiance, temperature and rainfall on PV yield is likely to be closely linked to the El Niño–Southern Oscillation ENSO cycle. To investigate this we use NREL's SAM model to simulate electricity production from a 3.275 megawatt pilot solar PV plant at the University of Queensland's Gatton Campus. A key finding was that the best simulated PV yields were obtained during 2013 and 2014 when ENSO neutral conditions but with an El Nino bias prevailed. The worst years were 2010 and 2011 which were characterised by moderate and weak La Nina phases of ENSO. All other years considered had average PV yield outcomes including 2015 which experienced a very strong El Nino event.

(1) INTRODUCTION

Economic assessment of the viability of solar PV farms depends crucially on the PV yield of these farms. In Australia, PV yield for utility scale solar PV farms will underpin revenue streams from: (1) merchant sale of electricity into the wholesale electricity market; (2) sale of eligible renewable energy certificates generated under the Large-scale Renewable Energy Target (LRET) scheme (CER, 2016); and (3) sale of electricity and sale or surrender of renewable energy certificates under PPA agreements with retail electricity companies. In principal, project viability requires that these revenue streams be sufficient to cover: (1) capital costs associated with the solar PV farm’s construction; (2) operation and maintenance expenditures linked to day to day operations of the solar farm; and (3) required return on invested capital.

In general, solar PV yield will depend on a number of different factors including: (1) solar irradiance and weather conditions; (2) soiling and shading effects; and (3) electrical losses associated with solar array infrastructure and the electricity network. In relation to weather conditions identified in the first point above, key variables will be ambient temperature and rainfall. The latter variable rainfall will play two potentially conflicting roles. First, rainfall will reduce levels of solar irradiance, especially direct beam solar irradiance, reducing PV yield. Second, rainfall will be a crucial factor in keeping PV modules clean, reducing module soiling and increasing PV yield harvested during non-rainy periods.

In Australia, the combined effects of weather relating to solar irradiance, temperature and rainfall on PV yield is likely to be closely linked to the El Niño–Southern Oscillation ENSO cycle (BOM, 2016). This paper will highlight some aspects of this interaction by simulating hourly PV yields using the US National Renewable Energy Laboratory’s (NREL) System Advisor Model (SAM) for years 2007-2015. These years capture different phases of the ENSO cycle and will enable assessment of how PV yield might vary with the different phases of ENSO. We will apply the PV simulations to The University of Queensland’s Gatton Solar Research Facility (GSRF) which is a 3.275 megawatt pilot solar PV plant.

The structure of this paper is as follows. The next section will give a brief description of the GSRF which underpins the modelling performed in this paper. Section 3 will contain a discussion of the approach utilised and critical requirements related to simulating PV yield of GSRF using the SAM model. Section 4 will contain a statistical analysis of simulated hourly solar PV yields of GSRF, including projections of annual solar PV yield for years 2016, 2017 and 2018 given currently available ENSO forecasts. The last section will contain conclusions.

(2) GSRF DESIGN AND LAYOUT

(2.1) Layout of GSRF

The GSRF is a solar pilot plant that comprises three different solar sub-array technologies: (1) a Fixed Tilt (FT) array comprising three identical 630 kW systems (UQ, 2015a); (2) a 630 kW Horizontal Single Axis Tracking (SAT) Array utilising First Solar's SAT system (UQ, 2015b); and (3) a 630 kW Dual Axis Tracker (DAT) utilising the Degertraker 5000 HD system (UQ, 2015c).

An overhead NearMap picture of the GSRF is documented in Figure 1. The three FT sub-arrays can be located, respectively, at the top right hand side (termed the 'Top' FT sub-array) and with the main FT sub-arrays being located just *below* the buildings and line of trees but *above* the road in Figure 1. For the purpose of this report, we split the main FT sub-into a *left hand side* sub-array (e.g. far left hand side part of the main FT array) and a *right hand side* sub-array which is that component directly in front of the UQ Solar Research facility in Figure 1. The FT system design has the following technical design features:

- All modules have a tilt angle of 20 degrees; and
- All modules have an azimuth angle of 357 degrees (e.g. modules are facing in the direction of three degrees west of north).

The SAT sub-array can be located in Figure 1 immediately below the top FT sub-array, adjacent to the main FT sub-arrays and also *above* the road in Figure 1. The SAT sub-array has the following technical aspects:

- The sub-array is a horizontal array and thus has a tilt angle of 0 degrees;
- The sub-array has an azimuth angle of 357 degrees (e.g. same as the FT system);
- Maximum tracker rotation limit is set to 45 degrees; and
- No backtracking is implemented.

In Figure 1, the DAT sub-array is located underneath the main FT sub-arrays and *below* the road. There are 160 individual trackers installed at Gatton that are capable of a 340 degree slewing motion and a 180 degree tilt that allow the panels to directly face the sun at all times of the day, thereby maximising output.

The same First Solar CdTe FS-395 PLUS modules are installed on all five sub-arrays. There are in excess of 36,000 modules installed at GSRF across the five sub-arrays. The same type of inverter is also connected to each of the 630 kW sub-arrays and is a SMA Sunny Central 720CP XT inverter. Therefore, the whole array contains five inverters and through the current connection agreement with the local distribution network service provider Energex, each inverter's output is limited to 630 kW.

Figure 1. NearMap Picture of the GSRF Solar Array

(3) DESIGN INFORMATION USED IN SAM MODELLING

(3.1) Background

The SAM model (Gilman, 2015) was used to simulate the PV yield of the whole GSRF solar farm. Implementation of SAM modelling requires information relating to system design and size including information about: (1) number of modules in a string; (2) number of strings in parallel; and (3) the number of inverters. From this information as well as additional information supplied about modules and inverters, the following system information is determined: (1) maximum DC capacity of the solar array; (2) maximum DC input capacity of the inverters; and (3) maximum AC output capacity of the inverters. The key system design parameters and quantities used in the SAM simulations for each sub-array are reported in Table 1.

Table 1. Sub-array System Design Parameters

Description	Value	Measurement Unit
Modules per string	15	NA
Strings in parallel	480	NA
Number of inverters	1	NA
Configuration at reference conditions		
Modules:		
Nameplate capacity	685.901	kWdc
Number of modules	7,200	NA
Total module area	5,184	m^2
Total land area	4.3	acres
Inverters:		
Nameplate capacity – on output	630.000	kWac
Nameplate capacity – on input	638.945	kWdc

The modelling approach adopted for the complete solar farm was to model the whole array as five separate sub-arrays according to the design parameters listed in Table 1 and with separate near-object and diffuse shading factors for each individual sub-array. The system wide PV yield was then calculated as the sum of the PV yields of the five separate sub-arrays.

SAT tracking is implemented in SAM by setting the tilt angle to a pre-specified value (e.g. 0 degrees in our case) and having the tracking algorithm rotate the sub-array to track the azimuth angle of the sun's position, within limits set by the maximum tracker rotation limit (e.g. 45 degrees in our case). In the case of the DAT tracking algorithm, the tilt and azimuth angles of the tracking mechanism are set by the zenith and azimuth angles of the sun's position throughout the day (Gilman, 2015, Chapter 5.2).

(3.2) PV Yield Simulation Using the SAM Model

To run simulations in SAM, various user supplied inputs are required. These relate to: (1) hourly solar and weather data; (2) technical information about modules, inverters, array sizing and design; (3) soiling effects; (4) shading effects; and (5) DC and AC electrical losses. In the modelling performed for this paper, we also assumed that all modules, inverters and solar tracking infrastructure were in good working order.

Solar and weather data

The solar data was obtained from the Australian Bureau of Meteorology's (BOM) hourly solar irradiance satellite gridded data (BOM, 2015) whilst the weather data was sourced from the BOM's Automatic Weather Station (AWS) located at the University of Queensland's Campus at Gatton. Further details can be found in Wild (2016). Within SAM, the Perez Sky Diffuse model was used to determine Plane-of-Array (POA) irradiance (Gilman, 2015, Section 6.2).

Soiling effects

After solar irradiance and temperature, module soiling is generally regarded as the third most important factor determining solar PV yield (Gilman, 2015, Section 7.5). To assess the potential impact of soiling, three soiling scenarios were developed, termed 'low', 'medium' and 'high'. The determination of these particular soiling scenarios was linked to recorded daily rainfall over the period 2007 to 2015 at the nearby UQ Gatton Campus BOM AWS and assumed daily soiling rates applicable in the absence of daily rainfall. The soiling factors were also adjusted for local spectrum (see Wild (2016) for further details). For completeness, the monthly soiling factors employed for the three module soiling scenarios are reproduced in Table 2.

Table 2. Different augmented soiling rate configurations (Percentage)

Month	Low	Medium	High
Jan	0.0	0.0	0.0
Feb	0.1	0.5	1.8
Mar	0.3	0.5	1.1
Apr	1.2	2.0	4.3
May	2.3	4.4	8.2
Jun	2.4	4.0	6.7
Jul	3.6	7.0	9.5
Aug	3.7	6.8	10.6
Sep	3.2	6.6	12.5
Oct	2.5	5.2	10.5
Nov	0.9	1.4	2.5
Dec	0.3	0.4	0.9

Annualised Average	1.7	3.2	5.7

Shading effects

Solar PV yield assessment using SAM also requires that the effects of shading on modules be accounted for. Near-object shading can be interpreted as a reduction in POA incident irradiation by external objects located near to the array such as building and trees and is assumed to affect each sub-array uniformly. Account of near-shading effects is performed in SAM utilizing a three-dimensional representation of the sub-arrays and nearby external shading objects. Near-object shading affects both direct (beam) and diffuse POA irradiance (Gilman, 2015, Section 7.2).

The reduction in beam irradiance due to near-object shading is modelled by a set of hourly shading losses that reduce the plane-of-array beam solar irradiance in a given hour. The reduction in diffuse POA irradiance is modelled by a single sky diffuse loss percentage. In calculating the sky diffuse shading factor in SAM, an isotropic diffuse radiation model is assumed in which diffuse radiation is assumed to be uniformly distributed across the sky (Gilman, 2015, Section 7.2).

We utilised SAM's 3d shading calculator to determine both near object direct beam and constant sky diffuse shading losses for the five sub-arrays. The near object direct beam shading losses by hour and month determined for the five sub-arrays are reported in Table 3, Panels (A)-(E). The constant sky diffuse shading losses for each of the five sub-arrays are reported in Table 4.

In interpreting the percentage values listed in Table 3, values of 100 indicate complete shading. Values between 100 and zero per cent indicate partial shading with the extent of shading declining with the magnitude of the shading percentage value. Finally, a value of zero indicates no near-object shading effect.

Table 3. Direct beam near-object shading factors for Gatton sub-arrays (Percentage)

Panel (A): Left Hand Side Main FT sub-array

Month	5:00 AM	6:00 AM	7:00 AM	8:00 AM	9:00 AM	10:00 AM	11:00 AM	12:00 PM	1:00 PM	2:00 PM	3:00 PM	4:00 PM	5:00 PM	6:00 PM
JAN	100	0.0	0.0	0.0	0.0	0.0	0.0	0.0	0.0	0.0	0.0	0.0	0.0	100
FEB	100	0.0	0.0	0.0	0.0	0.0	0.0	0.0	0.0	0.0	0.0	0.0	0.0	100
MAR	100	0.0	0.0	0.0	0.0	0.0	0.0	0.0	0.0	0.0	0.0	0.0	0.0	100
APR	100	11.7	0.0	0.0	0.0	0.0	0.0	0.0	0.0	0.0	0.0	0.0	67.0	100
MAY	100	83.5	4.7	0.0	0.0	0.0	0.0	0.0	0.0	0.0	0.6	36.5	100	100
JUN	100	100	39.6	1.2	0.0	0.0	0.0	0.0	0.0	0.1	3.9	56.1	100	100
JUL	100	100	33.6	0.6	0.0	0.0	0.0	0.0	0.0	0.0	1.3	42.3	100	100
AUG	100	94.7	0.1	0.0	0.0	0.0	0.0	0.0	0.0	0.0	0.0	2.8	100	100
SEP	100	0.0	0.0	0.0	0.0	0.0	0.0	0.0	0.0	0.0	0.0	0.0	14.7	100
OCT	100	0.0	0.0	0.0	0.0	0.0	0.0	0.0	0.0	0.0	0.0	0.0	0.0	100
NOV	0.0	0.0	0.0	0.0	0.0	0.0	0.0	0.0	0.0	0.0	0.0	0.0	0.0	100
DEC	100	0.0	0.0	0.0	0.0	0.0	0.0	0.0	0.0	0.0	0.0	0.0	0.0	100

Panel (B): Right Hand Side Main FT sub-array

Month	5:00 AM	6:00 AM	7:00 AM	8:00 AM	9:00 AM	10:00 AM	11:00 AM	12:00 PM	1:00 PM	2:00 PM	3:00 PM	4:00 PM	5:00 PM	6:00 PM
JAN	100	0.5	0.3	0.1	0.0	0.0	0.0	0.0	0.0	0.0	0.1	0.3	0.6	100
FEB	100	0.8	0.3	0.1	0.1	0.1	0.0	0.0	0.1	0.1	0.1	0.1	0.8	100
MAR	100	0.8	0.5	0.3	0.2	0.1	0.1	0.1	0.1	0.2	0.3	0.4	1.2	100
APR	100	13.0	0.5	0.3	0.2	0.1	0.1	0.1	0.2	0.2	0.3	2.5	80.5	100
MAY	100	83.7	6.1	0.4	0.2	0.2	0.2	0.2	0.2	0.6	4.7	60.7	100	100
JUN	100	100	29.4	2.2	0.3	0.2	0.2	0.3	0.6	2.1	15.9	76.1	100	100
JUL	100	100	25.3	1.6	0.3	0.2	0.2	0.2	0.4	1.0	8.1	65.4	100	100
AUG	100	72.9	1.3	0.3	0.2	0.2	0.2	0.2	0.2	0.2	0.6	14.8	100	100
SEP	100	1.1	0.4	0.2	0.1	0.1	0.1	0.1	0.1	0.2	0.3	0.6	19.9	100
OCT	100	0.6	0.2	0.2	0.1	0.1	0.1	0.1	0.1	0.2	0.3	0.3	1.9	100
NOV	1.3	0.4	0.2	0.0	0.0	0.0	0.0	0.0	0.0	0.1	0.1	0.5	1.0	100
DEC	100	0.5	0.3	0.1	0.0	0.0	0.0	0.0	0.0	0.0	0.1	0.4	0.7	100

Panel (C): Top FT sub-array[1]

Month	5:00 AM	6:00 AM	7:00 AM	8:00 AM	9:00 AM	10:00 AM	11:00 AM	12:00 PM	1:00 PM	2:00 PM	3:00 PM	4:00 PM	5:00 PM	6:00 PM
JAN	100	0.0	0.0	0.0	0.0	0.1	0.1	0.1	0.3	0.1	0.0	0.0	0.0	100
FEB	100	0.0	0.0	0.2	0.8	0.9	0.6	0.6	1.0	1.2	1.1	0.2	0.0	100
MAR	100	0.0	3.3	3.4	2.6	2.4	1.4	1.4	2.2	2.9	4.2	6.5	34.8	100
APR	100	60.8	14.0	6.8	4.0	3.6	2.2	2.5	3.8	5.4	8.2	23.1	83.7	100
MAY	100	79.4	61.9	17.2	8.0	6.5	4.6	5.4	7.3	11.6	17.9	46.7	100	100
JUN	100	100	81.8	33.6	13.3	9.5	7.0	7.7	10.4	17.0	24.0	46.3	100	100
JUL	100	100	85.0	29.9	11.8	8.2	6.2	6.3	8.6	13.8	19.5	43.3	100	100
AUG	100	71.5	41.8	11.5	5.9	5.0	3.3	3.5	5.2	7.3	11.1	37.3	100	100
SEP	100	8.0	6.7	4.8	3.0	2.8	1.6	2.1	3.0	3.9	6.0	10.2	92.7	100
OCT	100	0.0	0.8	1.6	1.6	1.4	0.7	1.2	1.7	2.2	2.5	1.4	39.8	100
NOV	0.0	0.0	0.0	0.0	0.2	0.3	0.1	0.3	0.5	0.3	0.0	0.0	4.1	100
DEC	100	0.0	0.0	0.0	0.0	0.0	0.0	0.1	0.1	0.0	0.0	0.0	0.0	100

[1] The shading percentages reported in Panel (C) for the top FT sub-array reflect the impact of two trees that were in very close proximity to the sub-array. These trees have very recently been cut down so the shading effects outlined in Panel (C) would now overstate the extent of near-object shading.

Panel (D): SAT sub-array

Month	5:00 AM	6:00 AM	7:00 AM	8:00 AM	9:00 AM	10:00 AM	11:00 AM	12:00 PM	1:00 PM	2:00 PM	3:00 PM	4:00 PM	5:00 PM	6:00 PM
JAN	3.5	0.0	0.0	0.0	0.0	0.0	0.0	0.0	0.0	0.0	0.0	0.0	0.0	5.2
FEB	100	0.0	0.0	0.0	0.0	0.0	0.0	0.0	0.0	0.0	0.0	0.0	0.0	3.6
MAR	100	0.0	0.0	0.0	0.0	0.0	0.0	0.0	0.0	0.0	0.0	0.0	0.0	100
APR	100	0.0	0.0	0.0	0.0	0.0	0.0	0.0	0.0	0.0	0.0	0.0	39.7	100
MAY	100	5.3	0.0	0.0	0.0	0.0	0.0	0.0	0.0	0.0	0.0	34.2	100	100
JUN	100	100	8.8	0.0	0.0	0.0	0.0	0.0	0.0	0.0	0.5	53.2	100	100
JUL	100	100	5.1	0.0	0.0	0.0	0.0	0.0	0.0	0.0	0.0	31.5	100	100
AUG	100	0.7	0.0	0.0	0.0	0.0	0.0	0.0	0.0	0.0	0.0	1.4	100	100
SEP	100	0.0	0.0	0.0	0.0	0.0	0.0	0.0	0.0	0.0	0.0	0.0	32.4	100
OCT	0.8	0.0	0.0	0.0	0.0	0.0	0.0	0.0	0.0	0.0	0.0	0.0	0.0	100
NOV	0.0	0.0	0.0	0.0	0.0	0.0	0.0	0.0	0.0	0.0	0.0	0.0	0.0	100
DEC	0.1	0.0	0.0	0.0	0.0	0.0	0.0	0.0	0.0	0.0	0.0	0.0	0.0	10.9

Panel (E): Direct beam shading factors: representative DAT sub-array

Month	5:00 AM	6:00 AM	7:00 AM	8:00 AM	9:00 AM	10:00 AM	11:00 AM	12:00 PM	1:00 PM	2:00 PM	3:00 PM	4:00 PM	5:00 PM	6:00 PM
JAN	8.8	2.2	0.7	0.2	0.0	0.0	0.0	0.0	0.0	0.0	0.0	0.0	0.0	0.0
FEB	100	3.1	0.8	0.0	0.0	0.0	0.0	0.0	0.0	0.0	0.0	0.0	0.0	0.0
MAR	100	2.5	0.0	0.0	0.0	0.0	0.0	0.0	0.0	0.0	0.0	0.0	0.0	100
APR	100	5.6	0.0	0.0	0.0	0.0	0.0	0.0	0.0	0.0	0.0	0.0	0.0	100
MAY	100	15.1	0.0	0.0	0.0	0.0	0.0	0.0	0.0	0.0	0.0	0.0	100	100
JUN	100	100	0.0	0.0	0.0	0.0	0.0	0.0	0.0	0.0	0.0	0.0	100	100
JUL	100	100	0.0	0.0	0.0	0.0	0.0	0.0	0.0	0.0	0.0	0.0	100	100
AUG	100	13.6	0.0	0.0	0.0	0.0	0.0	0.0	0.0	0.0	0.0	0.0	100	100
SEP	100	0.0	0.0	0.0	0.0	0.0	0.0	0.0	0.0	0.0	0.0	0.0	0.0	100
OCT	5.0	1.7	0.0	0.0	0.0	0.0	0.0	0.0	0.0	0.0	0.0	0.0	0.0	100
NOV	7.5	1.5	0.5	0.0	0.0	0.0	0.0	0.0	0.0	0.0	0.0	0.0	0.0	100
DEC	7.8	1.8	0.6	0.0	0.0	0.0	0.0	0.0	0.0	0.0	0.0	0.0	0.0	0.0

In general, the DAT sub-array (Panel E) has the lowest shading impacts in the early morning and early evening hours when compared to the shading effects of both the FT and SAT sub-arrays. The SAT sub-array (Panel D) has the next lowest shading impacts with the FT sub-arrays experiencing the highest near object shading effects. Note that this outcome was also observed in the constant sky diffuse shading loss percentages reported in Table 4. Of particular interest for PV yields projections is that the main FT sub-arrays (e.g. Panels A and B) experience very little or no near object direct beam shading over the period 9 AM to 2 PM. However, in the case of the Top FT array (Panel C), shading effects occur throughout the day reflecting the close proximity of two trees near to this sub-array. In contrast, the representative SAT and DAT sub-arrays (Panels D and E) experience very little or no near object direct beam shading over slightly broader time horizons of 8 AM to 3 PM and 7 AM to 4 PM, respectively.

Table 4. Diffuse Shading Factors for Gatton sub-arrays (Percentage)

Sub-array	Diffuse Shading factor
LHS Main FT	4.45
RHS Main FT	5.80
Top FT	7.19
SAT	1.96
DAT	1.10

In the SAM modelling, self-shading was directly implemented for the three FT sub-arrays as well as for the SAT sub-array (Gilman, 2015, Section 7.3 and Chapter 8). The design settings adopted for self-shading analysis are listed in Table 5. For each FT sub-array, the basic design structure encapsulated ten rows of panels, with each row containing four modules stacked vertically on top of each other in landscape orientation. The number of modules in each row was 180. The row spacing between each row was 4.27 meters.

In the case of the SAT array, there are 30 rows with 4 modules stacked vertically on top of each other in landscape orientation. The number of modules along the bottom of each row is 60. The row spacing between each row is 7.30 meters.

Because the modules used in all five sub-arrays are thin film First Solar FS-395 PLUS modules, we employ the thin film linear shading option in SAM to model self-shading effects. This option is for specially-designed thin film modules with cells and bypass diodes wired in such a way that the modules output varies linearly with shaded area of the module. More generally, we found that incorporating self-shading in the PV Yield analysis for the FT and SAT sub-arrays had the effect of reducing total output by a *tenth* of one per cent for the FT sub-array and by around one per cent for the SAT array. Details of self-shading losses experienced for the SAT array by both soiling scenario and year (over the period 2007-2015) can be discerned from Panel (A) of Table 6.

Table 5. Self-shading Design Settings Used In SAM Modelling

Design Feature	FT sub-array	SAT sub-array
Number of modules along the side of row	4	4
Number of modules along the bottom of row	180	60
Number of rows	10	30
Shading algorithm	Thin film (linear)	Thin film (linear)
Module orientation	Landscape	Landscape
Length of side (in meters)	1.69	1.69
Ground coverage ratio (%)	0.37	0.23
Row spacing (in meters)	4.27	7.30

The reason why self-shading losses are greater for the SAT array is that it can rotate to track the azimuth angle of the sun, thereby producing greater yield in the early morning and early evening hours when self-shading effects are most prevalent. Thus, the reduction in output due to self-shading is greater in the case of the SAT array when compared with the FT array whose azimuth (and tilt) angle are fixed throughout the day. As a result, the system cannot track the sun's position, thus implying much lower levels of POA irradiance for FT arrays when self-shading effects principally arise.

Unfortunately, self-shading effects are not currently calculated in SAM for the DAT array. Therefore, we attempted to loosely approximate these losses by applying the self-shading weights determined by hour, month and year for the SAT system to PV yields given the near-object and diffuse shading factors specific to the GSRF DAT sub-array. This approach would have some worth to the extent that the timing of self-shading effects is likely to coincide for both the SAT and DAT sub-arrays. However, because both the row spacing and orientation will be different for the DAT sub-array, the actual shading factors will likely be significantly different to those calculated for the SAT sub-array.

In general, we would expect self-shading losses for the DAT array to be magnified further because both the tilt and azimuth angles of the DAT array track the sun's zenith and azimuth angles over the day. Thus, both tilt and azimuth tracking would be expected to improve the POA irradiance of the array over the competing FT and SAT arrays. As such, we would expect the DAT array to be more susceptible to larger output reductions in the early morning and evening hours when self-shading effects are most prevalent. Support for this proposition can be found in the results presented in Panel (B) of Table 6 which shows average self-shading losses by year when the hourly self-shading loss factors of the SAT array are applied to the output of the DAT array. In this case, the self-shading losses for the DAT array are around 3.5 per cent across all three soiling scenarios. This result can be contrast with the equivalent result for the SAT sub-array of 1 per cent.

Table 6. Self-shading Losses (%) by Array Tracking Type and Soiling Scenario

Panel (A): SAT Array

Year	Low soiling	Medium soiling	High soiling
2007	-1.10	-1.10	-1.10
2008	-1.14	-1.14	-1.15
2009	-1.14	-1.14	-1.14
2010	-1.06	-1.06	-1.06
2011	-0.97	-0.97	-0.97
2012	-1.01	-1.01	-1.01
2013	-1.15	-1.14	-1.14
2014	-1.02	-1.01	-1.02
2015	-0.67	-0.67	-0.67
Average	-1.03	-1.03	-1.03

Panel (B): DAT array

Year	Low soiling	Medium soiling	High soiling
2007	-3.55	-3.55	-3.55
2008	-3.57	-3.57	-3.57
2009	-3.57	-3.57	-3.58
2010	-3.55	-3.54	-3.54
2011	-3.50	-3.50	-3.50
2012	-3.38	-3.37	-3.36
2013	-3.55	-3.54	-3.54
2014	-3.46	-3.45	-3.45

2015	-3.06	-3.07	-3.08
Average	-3.47	-3.46	-3.46

Module and Inverter Information

Details relating to module and inverter information employed in the SAM modelling remain the same as discussed in Wild (2016). Recall that the modules used at GSRF are First Solar CdTe FS-395 PLUS modules and each of the five sub-arrays is connected to SMA Sunny Central 720CP XT inverter with operational sent-out capacity restricted to 630 kW through the current connection agreement.

For completeness, the parameter settings required for the SAM simulations for modules and inverters are listed in Panels (A) and (B) of Table 7, respectively

Table 7. SAM Module and Inverter Parameter Settings

Panel (A): Modules

Description	Value	Measurement Unit
Module description - Thin Film Cadmium Telluride module	First Solar FS-395 PLUS	NA
Cell type – CdTe	NA	NA
Module area	0.72	m^2
Nominal operating cell temperature	45	°C
Maximum power point voltage (Vmp)	45.8	V
Maximum power point current (Imp)	2.08	A
Open circuit voltage (Voc)	58	V
Short circuit current (Isc)	2.29	A
Temperature coefficient of Voc	-0.28	%/°C
Temperature coefficient of Isc	0.04	%/°C
Temperature coefficient of maximum power point	-0.29	%/°C
Number of cells in series	146	NA
Standoff height	Ground or rack mounted	NA
Approximate installation height	one story building height or lower	NA

Panel (B): Inverters

Description	Value	Measurement Unit
Inverter type	SMA Sunny Central 720CP XT	NA
Maximum AC power output	630,000	Wac
Manufacturer efficiency	98.6	%
Maximum DC input power	638,945	Wdc
Nominal AC voltage	324	Vac
Maximum DC voltage	1000	Vdc
Maximum DC current	1400	Adc
Minimum MPPT DC voltage	577	Vdc
Nominal DC voltage	577	Vdc
Maximum MPPT DC voltage	850	Vdc
Power consumption during operation	1950	Wdc
Power consumption at night	100	Wac

DC and AC Losses

Details relating to DC and AC losses employed in the SAM modelling also remain the same as discussed in Wild (2016). Thus, values for derating DC array output associated with DC electrical losses of between 3.56 and 3.99 per cent were adopted, depending upon the array technology, together with AC electrical losses of 2.14 per cent. Details of specific settings are listed in Table 8.

Table 8. DC and AC Electrical Losses Used in SAM Modelling

Description	FT Value (%)	SAT Value (%)	DAT Value (%)
DC Array Losses			
Mismatch	1.1	1.1	1.1
Diodes and connections	0.0	0.0	0.0
DC wiring	1.5	1.5	1.5
DC tracking losses	0.0	0.45	0.42
Nameplate DC power loss	1.0	1.0	1.0
DC power optimisation	0.0	0.0	0.0
Total DC losses	3.56	3.99	3.96
AC System losses			
AC wiring	1.0	1.0	1.0
Transformer losses	1.15	1.15	1.15
Total AC Losses	2.14	2.14	2.14

It should be noted that the DC ‘Mismatch’ and ‘Nameplate’ loss factors were partially reduced to ensure that net losses were zero when the modification were made to ensure that the augmented soiling loss factors adjusted for local spectrum reported in Table 2 were non-negative.

(4) STATISTICAL ANALYSIS OF SOLAR PV YIELD SIMULATION OF GSRF

(4.1) Hourly and Annual PV Yield Projections for 2007-2015

The SAM model was used to simulate PV yields for the whole Gatton array using the near-object and self-shading loss percentages reported in Tables 3 to 6 and augmented soiling losses outlined in Table 2 for the three particular soiling scenarios: (1) low; (2) medium; and (3) high. The annualised total PV yields of the whole solar farm and for the period 2007-2015 are reported in Table 9 for each soiling scenario. It should be noted that because of satellite problems, solar irradiance data was missing from the BOM’s hourly solar irradiance dataset for: (1) year 2008, 14 to 17 of March and 10-13 of April; and (2) year 2009, 17-18 of February, 12 and 16-27 of November. Thus, the annual production totals reported in Table 9 for years 2008 and 2009 will be understating the true annual production levels as a result of this missing data. Moreover, both the annual production data reported in Table 9 and the Typical Meteorological Year (TMY) calculations reported below are based on the hourly solar PV yields generated from SAM model simulations for years 2007 to 2015, assuming 365 days in each year. Hence the extra day (e.g. 29 February) has been dropped for leap years 2008 and 2012.

Inspection of Table 9 indicates that for the period 2007-2015, the best year for solar PV yield was 2014, followed by years 2013 and 2012. These years were categorised as ENSO neutral but with an emerging strong El Nino bias. Interestingly and somewhat surprisingly, 2015 with its very strong El Nino pattern reverted back to a more average PV yield, suggesting a complicated relationship between El Nino strength and PV yield.

Other good years were 2007 and 2009, especially when accounting for the missing data in the latter case. Year 2007 can be classified as involving a transition from a weak El Nino pattern through the first half of 2007 into a moderate strength La Nina pattern over the second half of 2007. Year 2009, in turn, can be classified as transitioning from ENSO neutral conditions during the first half of 2009 into a moderate strength El Nino over the second half of 2009 (Null, 2016).

The other very noticeable feature in Table 9 is the noticeably lower annual PV yields over years 2010 and 2011. These particular years involved a transition from a moderate strength El Nino pattern over the first half of 2010 into a moderate strength La Nina over the second half of 2010 and first half of 2011 before evolving into a weaker La Nina pattern over the remainder of 2011 (Null, 2016).

Table 9. Annual Solar PV Yield Projections (MWh's) from SAM Simulations by Soiling Scenario

	Soiling scenario		
Year	low	medium	high
2007	6586	6499	6352
2008	6439	6354	6208
2009	6497	6406	6254
2010	5787	5710	5581
2011	6235	6151	6010
2012	6591	6504	6355
2013	6790	6702	6550
2014	6907	6816	6662
2015	6499	6417	6276
Average	6481	6395	6250
% Change		-1.3	-3.6

The average annual PV yield calculated from the annual results reported for years 2007-2015 in Table 9 are listed in the second last row of that table. Across the three soiling scenarios considered, the average annual PV yield falls in the range of 6250 to 6481 MWh's. Annual average solar PV yield also declines as the degree of module soiling increases. The last row of Table 9 reports the percentage change in average annual PV yield for medium and high soiling relative to the average annual PV yield associated with low soiling. We see percentage *reductions* in average annual PV yield of 1.3 and 3.6 per cent, respectively, for the medium and high soiling scenarios relative to the low soiling scenario's average annual PV yield.

(4.2) Empirical Distribution Functions of Hourly PV Yields and TMY Calculations

We also used the hourly PV yields for years 2007 to 2015 as source data for TMY analysis. This was implemented by stacking each year's 8760 hourly PV yields across the top of a spreadsheet in chronological order commencing with 2007 and moving column-wise across the spreadsheet for years 2008 to 2015. We then calculated various statistical thresholds of interest, including minimum, maximum, average, median, and elsewhere incrementing by a percentile range of ten percentage points. That is, we calculated the 10^{th}, 20^{th}, 30^{th} percentiles of the column-wise stacked 2007-2015 hourly PV yield data, continuing up to the 80^{th} and 90^{th} percentiles. Of course, the minimum and maximum corresponds to the zero and 100^{th} percentile while the median correspond to the 50^{th} percentile. In statistical parlance, these percentiles would also give us the 100%, 90% 80%,…, 20%, 10% and 0% probabilities of exceedance (POE) results respectively. Note that applying each of these statistical thresholds would give a series of 8760 values corresponding to each hour in a year.

To determine the empirical distribution functions of the data corresponding to these statistical thresholds, we calculated the absolute value of the difference between the sequence of hourly threshold values and hourly production values of each year and aggregated these differences values over each individual month for each year in the interval 2007-2015. Note that the month of PV yield (e.g. production) data of a year that is the closest statistical match to the monthly data associated with each respective statistical threshold would have the *lowest* magnitude associated with the monthly summed difference values. For each statistical threshold mentioned above, the choice of month and year with the closest statistical match are reported in Table 10.

It is apparent from Table 10 that the monthly results jump around quite markedly although 2010 and 2011 tend to dominate in relative terms for lower statistical threshold levels (e.g. minimum, 90% POE and 80% POE thresholds). In contrast, 2013 and 2014 tend to dominate in relative terms for the higher threshold levels (e.g. 20% POE, 10% POE and maximum thresholds). For the mid-range thresholds (e.g. encompassing the range of 70% POE to 40% POE), years 2007, 2009 and 2012 appear to have relative prominence.

Using the year/month information reported in Table 10, we can 'pull out' the relevant month and year data records from the original SAM simulations underpinning the results in Table 9 and construct artificial annual data series consistent with these particular statistical threshold levels. This data will have 8760 individual hourly data points by construction. We then aggregate this hourly data over the year in order to derive annual production totals (in MWh's) and annual capacity factors (ACF's) consistent with each statistical threshold and soiling scenario. Note that in all cases, the ACF's are calculated against an energy sent-out maximum capacity of 3.15 MW. These results are reported in Table 11, Panels (A)-(C).

Examination of Table 11 indicates that for each respective statistical threshold level the production totals and ACF's both decline as the extent of module soiling increases. Moreover, as we move from lower to higher statistical thresholds [e.g. from Panels (A) to (C)], the production totals and ACF values increase across all the soiling scenarios. The range of the annualised production aggregates across both statistical threshold level and soiling scenario commences in the range of 5130 to 5327 MWh's (for the minimum statistical threshold) and increases in range to 7112 to 7369 MWh's associated with the maximum statistical threshold. Moreover, the ACF values increase from the lower-range band of 18.6 to 19.3 per cent to the upper-range band of 25.8 to 26.7 per cent.

Note that the average and median values for productions aggregates also differ quite markedly with the median values of 6716 to 6965 MWh's being well above the average values of 6330 to 6573 MWh's. This indicates that the empirical distribution function of the hourly PV yields over years 2007 to 2015 is left skewed – i.e. it has a much longer left hand side tail. The bunching of observations in the upper tail of the empirical distribution function is also indicated by the fact that the production results in Table 11 and year/month details in Table 10 coincide for both the 10% POE and maximum statistical threshold levels.

In Table 12, we cross-match the closest statistical threshold annual production values to the yearly simulated production totals that were reported in Table 9 using red shading and an 'X' symbol. From this table, it is clear that most years in the interval 2007-2015 are closest to the production total corresponding to the average statistical threshold. Once again, reflecting the observed left skewness of the empirical distribution function of the hourly PV yields, this particular threshold falls well to the left of the median statistical threshold, lying between the 70% POE and 60% POE statistical threshold levels. This means, in statistical terms, that the best estimate we have for annual PV yield under normal conditions would be between 6330 and 6573 MWh (depending upon soiling) or equivalently, between 22.9 and 23.8 per cent ACF.

For worse than normal conditions, the best estimate would be between the 80% POE and 70% POE thresholds giving a range for annual PV yield of between 5805 to 6223 MWh, or equivalently, between 21.0 to 22.6 per cent ACF. Furthermore, from analysis of PV yield over 2007-2015, these latter type of results are most likely to be linked to moderate or strong La Nina weather patterns with the worst outcomes more likely to be associated with stronger La Nina patterns.

For better than normal conditions, the best estimate for annual PV yield is likely to fall between the results associated with 60% POE and 50% POE (e.g. median) results. This points to an output range of 6531 to 6965 MWh's or equivalently, 23.7 to 25.2 per cent ACF. Once again, from analysis of PV yield over 2007-2015, the conditions that would seem to best support this type of result would be ENSO neutral conditions but with a strong El Nino bias. However, note that definite El Nino conditions do not seem to produce the best conditions for PV yield harvesting. For example, years with definitive El Nino weather patterns (e.g. broadly encompassing 2007, 2009 and 2015) produced average PV yields as documented in Table 12, notwithstanding the missing solar irradiance data in 2009. Also, only one year (e.g. 2014) produced PV yield outcomes that were consistent with the median yield calculated from our TMY methodology. Moreover, no simulated annual PV yield estimates relating to results in Table 9 corresponded to production levels *above* this median threshold.

The results above indicate that the best year for annual PV yield over the period 2007-2015 was year 2014 whose annual PV yield was only consistent with the annual output associated with the median statistical threshold. This implies, in turn, a 50 per cent chance of exceeding this result using data from the SAM PV simulations for the period 2007 to 2015. Furthermore, the annual PV production of other years lie below this statistical threshold with most of the annual results associated with the average statistical threshold. This latter threshold, falls between the 60 and 70 per cent probability of exceedance thresholds and implies that the simulated data could be re-organised to exceed these annual PV yields over 60 per cent of the time. This implies that for the 2007-2015 period we do not experience a consecutive run of good PV yielding months in any year to push the aggregate annual PV yield above the calculated median statistical threshold.

In order to see this, recall that the annual PV yield for 2014 was consistent with the median statistical threshold. However, in Table 10, in constructing the median threshold, only three months of 2014 were used – April, October and December. Even for the 10% POE and maximum statistical thresholds in Table 10 associated with the highest statistical thresholds for annual PV yield, year 2014 (the best year) only contributes five months – January, February, June, October and November. The next best year 2013 contributes only two additional months, August and December. This means that five other months listed in Table 10 for these two statistical thresholds correspond to years other than 2014 and 2013. Thus, from the SAM simulated PV yields over years 2007-2015, it is potentially possible to significantly exceed the highest observed annual yield corresponding to year 2014 if the weather was accommodating enough to produce a significant run of consecutive high yielding months. However, this phenomenon was not been observed in any of the actual annual simulated PV yields cited in Table 9 for the interval 2007-2015.

Table 10. Year by Month Selections for Typical Meteorological Year (TMY) Calculations

Month	Min	90% POE	80% POE	70% POE	Average	60% POE	Median	40% POE	30% POE	20% POE	10% POE	Max
January	2011	2008	2009	2009	2009	2007	2007	2007	2007	2014	2014	2014
February	2008	2010	2010	2010	2007	2007	2007	2007	2007	2007	2014	2014
March	2010	2010	2010	2011	2011	2011	2007	2007	2007	2007	2007	2007
April	2011	2011	2009	2014	2014	2014	2014	2014	2014	2007	2007	2007
May	2013	2010	2012	2012	2012	2012	2012	2012	2008	2008	2008	2008
June	2012	2012	2012	2012	2012	2012	2012	2014	2014	2014	2014	2014
July	2010	2013	2015	2015	2009	2009	2009	2014	2014	2014	2007	2007
August	2011	2011	2011	2012	2012	2012	2012	2009	2009	2009	2013	2013
September	2010	2010	2012	2012	2012	2009	2009	2009	2009	2009	2009	2009
October	2010	2010	2007	2007	2012	2012	2014	2014	2014	2014	2014	2014
November	2009	2010	2010	2010	2011	2011	2011	2011	2014	2014	2014	2014
December	2010	2010	2007	2007	2007	2014	2014	2013	2013	2013	2013	2013

Table 11. Annual Solar PV Yield Projections for Total Gatton Array by Soiling Type and POE/Statistical Threshold

Panel (A) Lower range thresholds

	Minimum			90% POE			80% POE			70% POE		
Soiling	**Low**	**Medium**	**High**	**Low**	**Medium**	**high**	**Low**	**Medium**	**High**	**Low**	**Medium**	**high**
MWh Production	5327	5253	5130	5512	5438	5312	6032	5948	5805	6223	6136	5989
ACF (%)	19.3	19.0	18.6	20.0	19.7	19.2	21.9	21.6	21.0	22.6	22.2	21.7

Panel (B) Mid-range thresholds

	Average			60% POE			50% POE (Median)			40% POE		
Soiling	**Low**	**Medium**	**High**	**Low**	**Medium**	**high**	**Low**	**Medium**	**High**	**Low**	**Medium**	**high**
MWh Production	6573	6482	6330	6777	6685	6531	6965	6873	6716	7245	7151	6991
ACF (%)	23.8	23.5	22.9	24.6	24.2	23.7	25.2	24.9	24.3	26.3	25.9	25.3

Panel (C) Upper range thresholds

	30% POE			20% POE			10% POE			Maximum		
Soiling	**Low**	**Medium**	**High**	**Low**	**Medium**	**high**	**Low**	**Medium**	**High**	**Low**	**Medium**	**high**
MWh Production	7315	7220	7060	7345	7250	7089	7369	7274	7112	7369	7274	7112
ACF (%)	26.5	26.2	25.6	26.6	26.3	25.7	26.7	26.4	25.8	26.7	26.4	25.8

Table 12. Cross Classification of Annual Simulated Production Totals with POE Production Totals

Year	Min	90% POE	80% POE	70% POE	Average	60% POE	Median	40% POE	30% POE	20% POE	10% POE	Max
2007					X							
2008					X							
2009					X							
2010			X									
2011				X								
2012					X							
2013						X						
2014							X					
2015					X							

(4.3) ENSO Forecasts and PV Yield Prognoses for 2016, 2017 and 2018

Current ENSO Forecasts for the remainder of 2016

The most recent 2016 plume of model ENSO predictions for the mid-June 2016 period compiled by both the International Research Institute (IRI) for Climate and Society (2016) and NOAA-NCEP (2016) are reported in Panels (A) and (B) of Figure 2, respectively. Given the severity of the recent 2015-16 El Nino event, the current consensus of the weather models included in Figure 2, Panel (A) seem to be pointing to either ENSO neutral conditions with a strong La Nina bias (most likely) or a weak La Nina event during the second half of 2016. The former outcome is suggested by the dynamic average of the model plumes as indicated by the yellow line in Figure 2, Panel (A).

In Panel (B) of Figure 2, the CFS.v2 ensemble mean (e.g. the black dashed line) predicts a rapid transition to La Niña by the July-August-September (JAS) 2016 timeframe. However, the magnitudes of the negative SST anomalies in Panel (B) are larger than -1.0 and thus broadly point to ENSO neutral conditions with strong La Nina bias.

Finally, in Panel (C) of Figure 2, the latest forecast of the POAMA model of the BOM published on 22 May 2016 also tends to support ENSO neutral conditions with strong La Nina bias emerging over the remainder of 2016 (BOM, 2016). BOM (2016) also confirms the end of the current 2015-16 El Nino event with indicators now officially entering into the ENSO neutral phase of the ENSO cycle.

In summary, all three models: (1) IRI [Panel (A)]; (2) CFSv2 [Panel (B)]; and (3) POAMA [Panel (C)] generally point to ENSO neutral conditions but with a strong La Nina bias developing over the remainder of 2016. The models do not provide any further forecasts for the period beyond the December 2016 to February 2017 timeframe. Therefore, considerable uncertainty exists about both ENSO status and strength of any La Nina event that might emerge during 2017 and extending into 2018.

Figure 2. 2016 June 2016 ENSO Forecasts

Panel (A): IRI[2]

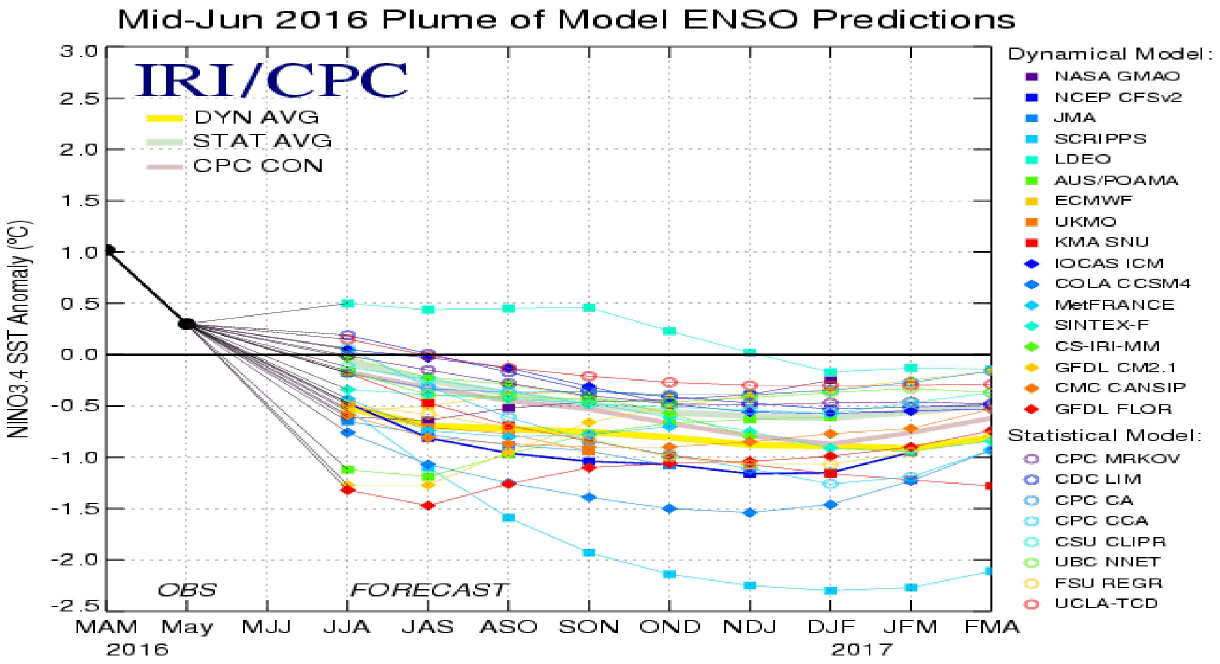

Panel (B): NOAA-NCEP

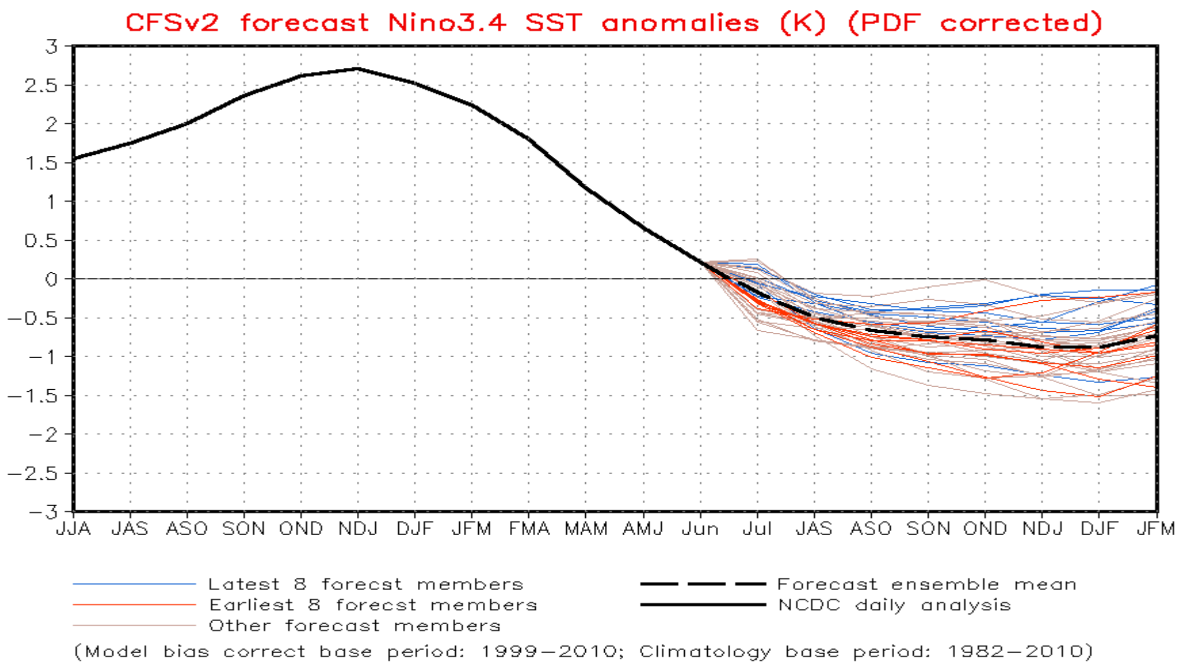

[2] This figure was sourced from: http://iri.columbia.edu/our-expertise/climate/forecasts/enso/current/ and updated on 16 June 2016 and accessed on 23-6-2016.

Panel (C): BOM-POAMA[3]

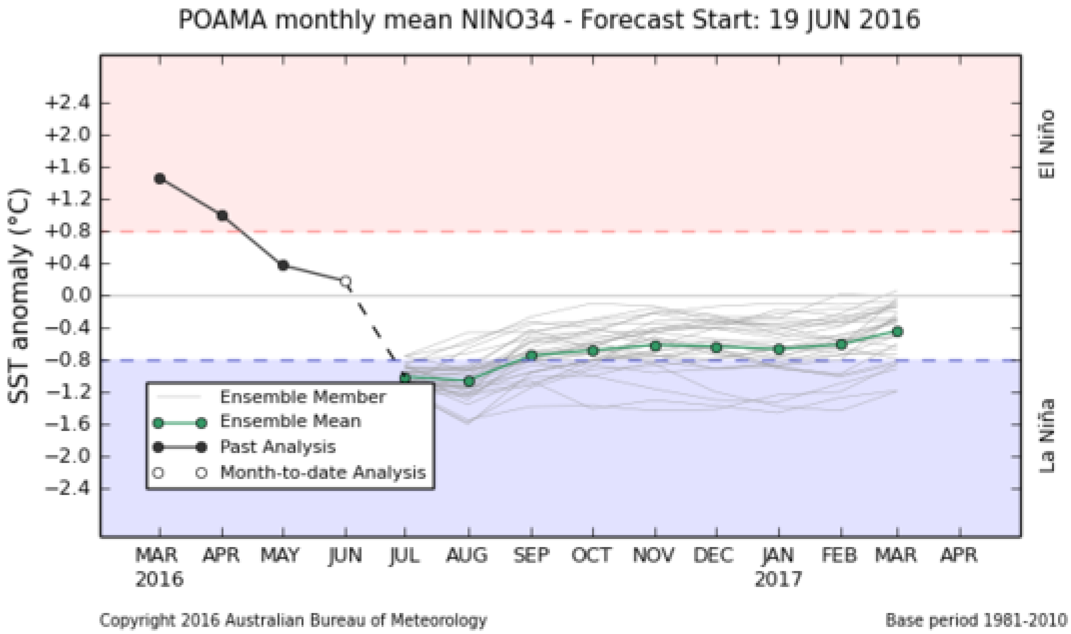

Projected Annual PV Yield: 2016

Given the 2016 ENSO forecasts mentioned above as well as the cross-matching between PV yields by year and statistical threshold highlighted in Table 12, the most likely prognosis (highlighted in red font below) is for annual PV yield in 2016 to fall in the band:

- 6330 to 6573 MWh if ENSO neutral conditions with a strong La Nina bias was to emerge over the remainder of 2016 (judged the most likely case); or

- 5989 to 6223 MWh if a weak La Nina event was to emerge over the remainder of 2016.

Discussion:

More generally, given the likelihood of either: (1) ENSO neutral with significant La Nina bias; or (2) very weak La Nina event arising over the remainder of 2016, we would expect total annual PV yield to fall within the average statistical threshold 6330 to 6573 MWh's band but with a downside risk to around 6223 MWh if a slightly stronger than expected La Nina pattern were to emerge during the remainder of 2016.

[3] This figure was sourced from http://www.bom.gov.au/climate/enso/#tabs=Outlooks. It was accessed on 23-6-2016.

Projected Annual PV Yield: 2017

The situation that ultimately arises in 2017 will significantly depend on what weather conditions prevail over the remainder of 2016. Initial guidance in Figure 2 indicates continuation of similar conditions to what emerged over 2016 – e.g. ENSO neutral conditions with strong La Nina bias or weak LA Nina conditions. However, some doubt exists over the potential strength of any La Nina event emerging during 2017. Overall, this would suggest the following conservative prognosis for PV yield in 2017:

- 6330 to 6573 MWh if ENSO neutral conditions with a strong La Nina bias emerge during 2017;
- 5989 to 6330 MWh if a weak La Nina event emerges during 2017 (judged the most likely case); or
- 5805 to 5989 MWh's if a moderate to strong La Nina event was to emerge during 2017.

Discussion:

One reason why the second band has been given the most weight is that unlike the situation arising in 2010 and 2011 when a moderate La Nina event emerged in 2010-11 followed by a weaker one in 2011-12, the reverse situation appears to be expected from the results identified in Figure 2. In particular, ENSO neutral conditions with a strong La Nina bias is currently expected to develop over the remainder of 2016 followed *potentially* by a weak La Nina event in 2017.

However, it should be recognised that considerable uncertainty surrounds the question of strength and ENSO status in 2017. Thus, we allow for downside risk to annual projected PV yield in the range of 5805 to 5989 MWh's in the case that either a moderate or strong La Nina event was to emerge in 2017. Similarly, we also account for a potential upside gain in projected annual PV yield in the range of 6330 to 6573 MWh's in the case that ENSO neutral conditions were to continue in 2017.

Projected Annual PV Yield: 2018

Longer term projections for 2018 would appear to suggest an ENSO neutral pattern if 2017 had either ENSO neutral or weak La Nina weather patterns or possibly a weak La Nina event if 2017 was characterised by moderate or strong La Nina weather patterns. Of these two cases, the most likely prognosis for longer term 2018 annual PV yield projection would be:

- 6330 to 6573 MWh if ENSO neutral conditions with La Nina bias or a weak La Nina event emerges during 2017 followed by ENSO neutral conditions in 2018 (judged the most likely case); or

- 5989 to 6330 MWh if a moderate to strong La Nina event emerges during 2017 followed by a weak La Nina event in 2018.

Discussion:

The above reasoning indicates the most likely range for annual PV yield in 2018 would be in the range 6330 to 6573 MWh's with perhaps a slight downside risk to around 6223 to 6330 MWh if a moderate or strong La Nina event had emerged in 2017.

For the convenience of readers, a summary of the above annual PV yield projections by year and according to: (1) most likely output range; (2) downside risk output range; and (3) upside gain output range, are reported in Table 13.

Table 13. Summary of 2016-2018 Projected Annual Solar PV Yield (MWh's)

Year/Comment	Most likely range (MWh's)	Downside risk (MWh's)	Upside gain (MWh's)
2016	6330 to 6573	6223 to 6330	N.A.
Comment	ENSO neutral with strong La Nina bias during second half of 2016	Weak La Nina event during second half of 2016	N.A.
2017	5989 to 6330	5805 to 5989	6330 to 6573
Comment	Weak La Nina event during 2017	Moderate to strong La Nina event during 2017	ENSO neutral with strong La Nina bias during 2017
2018	6330 to 6573	6223 to 6330	N.A.
Comment	ENSO neutral with strong La Nina bias during 2018	Weak La Nina event during 2018	N.A.

(5) CONCLUSIONS

Economic assessment of the viability of solar PV farms depends crucially on the PV yield of these farms. For utility scale solar PV farms, PV yield will underpin revenue streams available from the sale of electricity in wholesale market or through PPA contracts as well as from the sale of renewable energy certificates. Solar PV yield will depend on a number of different factors including solar irradiance and weather conditions, soiling and shading effects and electrical losses associated with both solar array infrastructure and the electricity network.

In Australia, the combined effects of weather relating to solar irradiance, temperature and rainfall on PV yield is likely to be closely linked to the El Niño–Southern Oscillation ENSO cycle. This paper investigated the interaction between PV yield and ENSO by simulating hourly PV yields using NREL's SAM for years 2007-2015 which captured different phases of the ENSO cycle. This modelling was applied to The University of Queensland's GSRF which is a 3.275 megawatt pilot solar PV plant. In modelling PV yields using the SAM model, different soiling regimes and near-object and self-shading effects were accounted for.

Hourly PV yields were simulated for years 2007 to 2015. These results indicated that the best simulated PV yields were obtained during 2013 and 2014 when ENSO neutral conditions with an emerging El Nino bias prevailed. The worst years for simulated PV yield were years 2010 and 2011 which were characterised by moderate and weak La Nina phases of ENSO, respectively. All other years considered had average PV yield outcomes. Interestingly, this also included 2015 which experienced a very strong El Nino suggesting a complicated relationship between El Nino strength and PV yield.

This hourly PV yield data was also used as source data for TMY analysis. In this approach, we effectively calculated the empirical distribution functions of this data for various statistical thresholds of interest. We then constructed artificial annual hourly PV yield data series on the basis of year/month choice that most closely approximated the statistical properties at these statistical thresholds. We then compared the annualised production outcomes from these artificial data series against those simulated for years 2007 to 2015 to classify the individual years against the statistical thresholds. The distribution of the simulated PV yields for years 2007-2015 were left skewed. For example, average statistical threshold fell between the 70% and 60% probability of exceedance thresholds whilst the median profile had, by definition, a 50% probability of exceedance. Most of the annual simulated PV yield totals for years 2007-2015 were matched closest to the production aggregate corresponding to the average statistical threshold. Annual PV yield during La Nina years were below normal, being consistent with PV yield profiles that had between 70% and 80% probability of exceedance. In contrast, the two best years were above normal, being consistent with PV profiles that had between 50% and 60% probability of exceedance. The best year 2014 was consistent with the median statistical threshold – e.g. had a 50% probability of exceedance profile.

It was also evident from the statistical analysis that the SAM simulated PV yields over years 2007-2015 could be re-ordered to potentially exceed the highest observed annual yield corresponding to year 2014 by a significant margin if the weather was accommodating enough to produce a significant run of consecutive high yielding months. However, this phenomenon was not observed in any of the actual simulated annual PV yields corresponding to the years in the interval 2007-2015.

PV yield projections were also developed for years 2016 to 2018 based upon the latest forecasts available for ENSO over the remainder of 2016 and statistical analysis of the hourly PV yields over 2007-2015. These forecasts indicated ENSO neutral conditions with a strong La Nina bias or weak La Nina patterns during the remainder of 2016. The status and strength of any potential La Nina event was more uncertain over the 2017-2018 timeframe. The bias towards the La Nina phase of ENSO suggested average to below average PV yields over the next couple of years with the most probable range falling within the 70% to average probability of exceedance range.

(6) REFERENCES

Bureau of Meteorology: BOM (2015) 'Australian Hourly Solar Irradiance Gridded Data.' Available at: http://www.bom.gov.au/climate/how/newproducts/IDCJAD0111.shtml.

Bureau of Meteorology: BOM (2016) 'ENSO Wrap-Up: ENSO outlooks.' Available at: http://www.bom.gov.au/climate/enso/#tabs=Overview. Accessed 23-6-2016.

Australian Government Clean Energy Regulator: CER (2016) 'Large-scale Renewable Energy Target.' Available at: http://www.cleanenergyregulator.gov.au/RET/About-the-Renewable-Energy-Target/How-the-scheme-works/Large-scale-Renewable-Energy-Target. Accessed 25-5-2016.

Gilman, P. (2015) 'SAM Photovoltaic Model Technical Reference.' National Renewable Energy laboratory (NREL), May. Available at: http://www.nrel.gov/docs/fy15osti/64102.pdf.

IRI (2016) 'International Research Institute (IRI) for Climate and Society, Earth Institute, Columbia University'. Available at: http://iri.columbia.edu/. Accessed 23-6-2016.

NOAA-NCEP (2016) 'ENSO: Recent Evolution, Current Status and Predictions Update prepared by: Climate Prediction Center / NCEP 20 June 2016.' Available at: http://www.cpc.ncep.noaa.gov/products/analysis_monitoring/lanina/enso_evolution-status-fcsts-web.pdf. Accessed 23-6-2016.

Null, J. (2016) 'El Niño and La Niña Years and Intensities.' Available at: http://ggweather.com/enso/oni.htm. Accessed 21-5-2016.

UQ (2015a) 'Fixed Tilt Array.' Available at: https://www.uq.edu.au/solarenergy/pv-array/content/fixed-tilt-array.

UQ (2015b) 'Single Axis tracking Array.' Available at: https://www.uq.edu.au/solarenergy/pv-array/content/single-axis-tracking-array.

UQ (2015c) 'Dual Axis tracking Array.' Available at: https://www.uq.edu.au/solarenergy/pv-array/content/dual-axis-array.

Wild, P. (2016a) 'Assessment of the Comparative Productive Performance of Three Solar PV Technologies Installed at UQ Gatton Campus Using the NREL SAM Model', GCI Clean Energy Discussion Papers June 2016, Discussion paper #5. Available at: http://gci.uq.edu.au/filething/get/11966/Assessment%20of%20economics%20of%20array%20types%20at%20gatton-SAM-FINAL.pdf.